

# Advancing Scalability and Sustainability of Perovskite Light-Emitting Diodes Through the Microwave Synthesis of Nanocrystals

Thais Caroline Almeida da Silva , Rafael S. Sánchez\* , Jaume-Adrià Alberola-Borràs ,  
Rosario Vidal , Iván Mora-Seró\* , and Beatriz Julián-López\* 

In recent years, perovskite light-emitting diodes have witnessed a remarkable evolution in both efficiency and luminance levels. Nonetheless, the production of such devices typically relies on protracted synthesis procedures at elevated temperatures and vacuum/inert conditions (e.g. hot-injection synthesis), thus rendering them technically unsuitable for extensive display and/or lighting applications manufacturing. Although alternative synthetic protocols have been proposed, e.g. ligand-assisted reprecipitation, ultrasonic and microwave-based methods, their suitability for the construction of high-performing light-emitting diodes has been reported in only a few studies. In this study, we demonstrate the fabrication of highly efficient lighting devices based on CsPbBr<sub>3</sub> colloidal perovskite nanocrystals synthesized by a fast, energetically efficient, and up-scalable microwave-assisted method. These nanocrystals exhibit an impressive photoluminescence quantum yield of 66.8% after purification, with a very narrow PL spectrum centered at 514 nm with a full width at half-maximum of 20 nm. Similarly, the PeLEDs achieve a maximum external quantum efficiency of 23.4%, a maximum current efficiency of 71.6 Cd A<sup>-1</sup>, and a maximum luminance level that exceeds 4.7 × 10<sup>4</sup> Cd m<sup>-2</sup>. Additionally, a significantly lower energy consumption for microwave-mediated synthesis compared with hot injection is demonstrated. These findings suggest that this synthetic procedure emerges as an outstanding and promising method towards a scalable and sustainable fabrication of high-quality perovskite light-emitting diodes.

## 1. Introduction

Research on perovskite nanocrystals (PeNCs) has garnered considerable attention over the last decade due to their narrow emission, tunable band gaps, tolerance to crystalline defects<sup>[1–3]</sup> and charge-carrier mobilities.<sup>[4–6]</sup> These attributes, combined with the ability of perovskite nanostructures to display extremely high photoluminescence quantum yields (PLQY),<sup>[7,8]</sup> have rendered them exceptionally promising for light-emitting applications. After the work of Mitzi and coworkers at the end of the last century,<sup>[9]</sup> interest in PeLEDs reemerged in 2014<sup>[10,11]</sup> following the interest in these materials for photovoltaic applications. Nowadays, substantial progress has been made towards enhancing the efficiency and overall performance of PeLEDs,<sup>[12–17]</sup> and in recent years, all-inorganic halide perovskites have provided significantly improved stability compared to their hybrid organic–inorganic counterparts.

Although several methodologies have been proposed for the synthesis of colloidal PeNCs,<sup>[18–23]</sup> the most successful traditional approach, namely hot-injection (HI) synthesis, entails sophisticated reaction setups involving a vacuum and inert atmosphere, elevated temperatures, and intricate procedures to yield high-quality PeNCs.<sup>[24–27]</sup> Unfortunately, these

requirements lead to elevated costs and insurmountable industrial implementation challenges. Instead, microwave-assisted (MW) synthesis presents numerous advantages, including selective heating, shorter reaction times, reduced energy consumption, industrially friendly implementation, and up-scalability. Microwave radiation indeed offers a more uniform heating profile, thus diminishing thermal gradients throughout the entire volume.<sup>[28,29]</sup> This uniform heating profile promotes consistent nucleation, which is a critical factor in the production of uniformly dispersed nanoparticles.<sup>[25]</sup> As a result, the MW method has gained widespread relevance in the preparation of both organic and/or inorganic perovskite derivatives,<sup>[30–33]</sup> although the suitability of the resulting PeNCs for the fabrication of functional devices remains unreported to date.

In this work, all-inorganic CsPbBr<sub>3</sub> PeNCs were prepared by modifying a MW approach that we recently reported<sup>[34]</sup> based on the pioneer

T. C. Almeida da Silva, Dr. R. S. Sánchez, Dr. J. Alberola-Borràs,  
Prof. I. Mora-Seró, Dr. B. Julián-López  
Institute of Advanced Materials (INAM), Universitat Jaume I, Av. Sos Baynat,  
s/n, 12071, Castelló de la Plana, Spain  
E-mail: [rasanche@uji.es](mailto:rasanche@uji.es)  
E-mail: [sero@uji.es](mailto:sero@uji.es)  
E-mail: [julian@qio.uji.es](mailto:julian@qio.uji.es)

Dr. J. Alberola-Borràs, Prof. R. Vidal  
Department of Mechanical Engineering and Construction, GID, Universitat  
Jaume I, Av. Sos Baynat s/n, 12071, Castelló de la Plana, Spain

 The ORCID identification number(s) for the author(s) of this article can be found under <https://doi.org/10.1002/eem2.12810>.

DOI: 10.1002/eem2.12810

works of Pan et al. and Liu et al.<sup>[31,32]</sup> In a typical experiment, cesium carbonate ( $\text{Cs}_2\text{CO}_3$ ), lead bromide ( $\text{PbBr}_2$ ), certain amounts of trioctylphosphine oxide (TOPO), oleic acid (OA), oleylamine (OLA), and 1-octadecene (ODE) were mixed in a 30 mL microwave quartz tube, which was then placed into a microwave reactor (Figure S1, Supporting Information). The reactor was then heated to 160 °C under 800 rpm to monitor the nucleation and growth evolution; see Supporting Information for more details.

## 2. Results and Discussion

The MW PeNCs were prepared at different reaction times. We discuss here the most interesting results for reaction times of 1, 3, and 7 min at 160 °C. Figure 1a–c shows the transmission electron microscopy (TEM) images of the monodisperse cube-like shaped  $\text{CsPbBr}_3$  NCs obtained through our approach. The average edge lengths of  $\text{CsPbBr}_3$  nanocubes are  $16.6 \pm 2.8$  nm,  $12.4 \pm 1.6$  nm, and  $9.7 \pm 1.5$  nm, for the samples obtained after 1, 3, and 7 min of reaction, respectively.

TEM images revealed that increasing the reaction time at 160 °C from 1 to 7 min consistently resulted in a decrease in particle size from approximately 17 to 10 nm, with a narrow size distribution (Figure S2, Supporting Information). This phenomenon is atypical, as in most synthetic procedures to obtain colloidal nanocrystals, the crystallization

kinetics can be described by the classical LaMer model,<sup>[35]</sup> commonly known as Ostwald ripening (OR),<sup>[36]</sup> in which the smaller particles in solution tend to dissolve and redeposit onto the larger ones, thereby promoting the growth of the particles over time. Conversely, our results show that for short reaction times (1–3 min), the formation of small PeNCs is restricted, thus resulting in larger particles. In fact, smaller sizes are achieved after longer reaction times (7 min). This fact indicates that the crystallization kinetics of PeNCs is governed by the reverse-Ostwald ripening (ROR), also known as digestive ripening,<sup>[37,38]</sup> which has recently gained attention in nanomaterials and perovskite synthesis studies.<sup>[36,39,40]</sup> The ROR involves the dissolution of large nanocrystals, often with some size polydispersity, towards the formation of smaller particles. Similar to MW synthesis, the fully controlled application of digestive ripening in semiconductor nanocrystals, particularly in the realm of colloidal perovskites, remains in its early stages. Therefore, this work aims to explore the key pathways and potential directions to achieve thorough control over the synthesis of PeNCs. It is worth mentioning that upon extending the reaction time to 10, 15, and 30 min, the formation of larger nanocrystals was again observed (Figure S3, Supporting Information), indicating that OR mechanisms predominate for lengthened reaction periods. Thus, the particle size of the PeNCs can be readily tailored from 9.7 to 17.3 nm through precise manipulation of the reaction time, similarly to other synthetic approaches.<sup>[41–44]</sup>

The crystalline structure of the sample prepared with 7 min-reaction time, shown in Figure 1d, was indexed to the orthorhombic  $\text{CsPbBr}_3$  structure with  $Pnmm$  space group as a single phase (ICSD 97851).<sup>[34,45,46]</sup> This crystalline phase is preferred by the system when perovskite nucleation occurs at relatively low temperatures,<sup>[43]</sup> contrary to hot-injection method in which cubic phase is usually obtained under thermodynamic conditions.<sup>[24]</sup> With our procedure, the orthorhombic crystallization can be attributed to a combined effect of a faster heating process and lower synthesis temperatures. Interestingly, both structures have direct energy bandgaps and possess similar optical properties<sup>[46]</sup> despite the variations in their lattice constants. The orthorhombic structure was further confirmed by the selected area electron diffraction (SAED) measurements (see Figure S4, Supporting Information). Elemental analyses by energy dispersive X-ray (EDX) spectroscopy confirmed the 1:1:3 atomic ratio for all the samples (Figure S5a–f, Supporting Information).

Figure 2a and Figure S6a,b, Supporting Information show the optical absorption and PL spectra of the  $\text{CsPbBr}_3$  PeNCs synthesized at 1, 3, and 7 min reaction times after the washing/purification procedure,<sup>[47]</sup> see Supporting Information for more details. The absorption spectra were normalized at the first excitonic peak ( $\lambda_{\text{abs}}^{\text{max}} \approx 497\text{--}498$  nm) and the emission spectra were normalized at their maxima ( $\lambda_{\text{em}}^{\text{max}} \approx 513\text{--}514$  nm). The optical curves were similar for all the samples. Only a 1 nm blue-shift in both the absorption edge and emission peak was detected

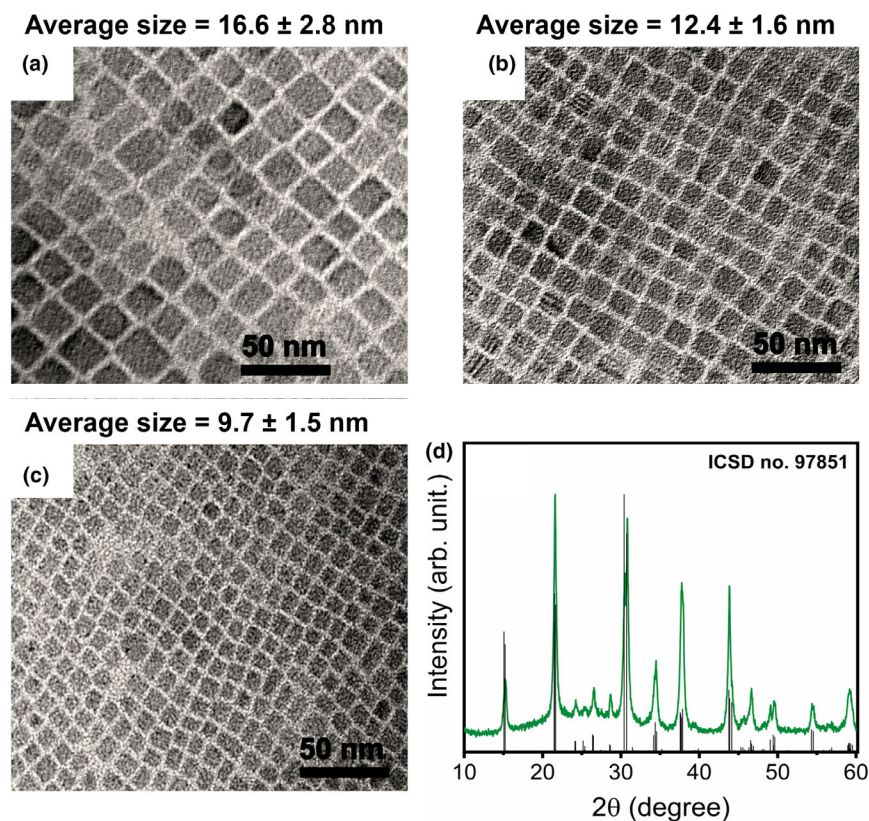


**Figure 1.** Morphological and crystallographic characterization: TEM images of the MW-synthesized  $\text{CsPbBr}_3$  PeNCs after different reaction times: a) 1 min; b) 3 min, and c) 7 min. The particle sizes were estimated upon analyzing more than 100 nanoparticles for each reaction time. d) XRD pattern of the sample synthesized after 7 min of reaction along with the simulated XRD pattern corresponding to the orthorhombic phase (ICSD 97851).

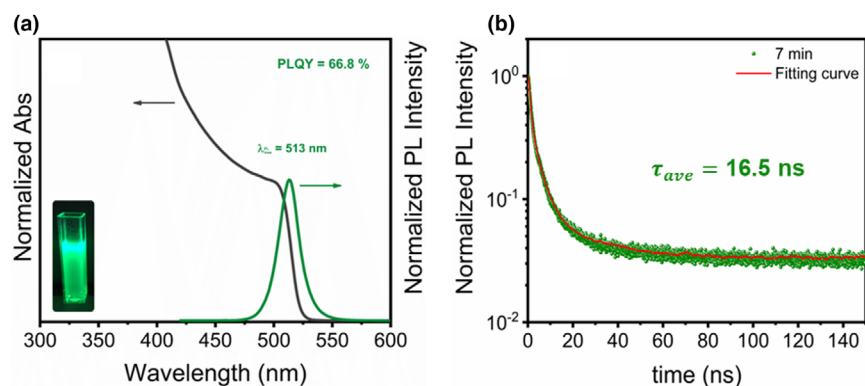


**Figure 2.** Optical characterization: a) UV-Vis absorption (black curve) and PL spectrum (green curve) of CsPbBr<sub>3</sub> NCs (7 min of reaction) in hexane with the PLQY value at  $\lambda_{\text{exc}} = 405$  nm; b) Time-resolved PL decay and the fitted curve for CsPbBr<sub>3</sub> NCs in hexane registered upon 405 nm excitation and 514 emission detection.

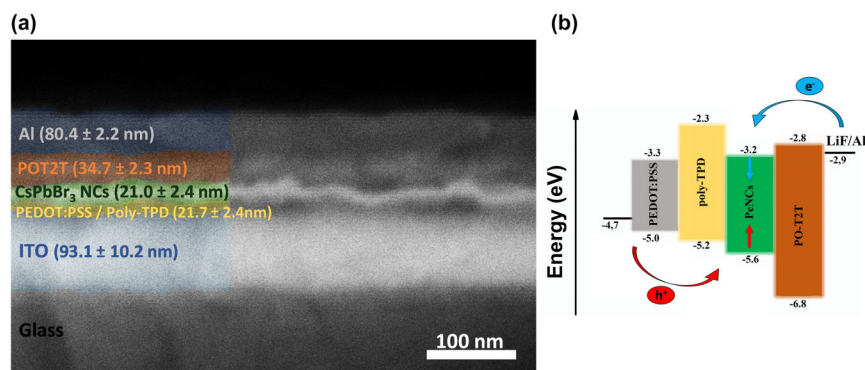


**Figure 3.** a) Cross-sectional image obtained via Scanning Electron Microscope (SEM) that displays the different stacked layers that constitute our PeLEDs with the corresponding thicknesses indicated in parentheses. b) Energy levels diagram of the different stacked materials that constitute the PeLEDs.<sup>[56]</sup>

for the sample with the smallest size, i.e. 9.7 nm average size (7 min reaction time). In the case of a strong-quantum confinement regime (below  $\sim 7$  nm<sup>[48,49]</sup>), and considering the definition of confinement energy ( $\Delta E = \hbar^2 \pi^2 / 2m^* r^2$ , where  $r$  is the particle radius and  $m^*$  is the reduced mass of the exciton), a substantial blue shift of the emission peak and absorption edge is expected when reducing the particle radius. According to our experimental observations, the optical properties are barely affected by the particle size, indicating that our NCs lie in the weak quantum confinement regime. Interestingly, due to the uniform particle size distribution, the emission spectra are very sharp, with narrow full width at half-maximum (FWHM) of 19.7, 18.7, and 20.4 nm for 1, 3, and 7 min-reaction time PeNCs, respectively.

The PeNCs solutions of the samples synthesized at 1, 3, and 7 min exhibited high PLQY values of  $42 \pm 4\%$ ,  $55 \pm 2\%$  and  $67 \pm 7\%$ , respectively, after purification. This purification process is very important to remove the excess of insulating organic molecules in the solution in order to fabricate high efficiency LEDs. These results demonstrate a positive correlation between the reduction of CsPbBr<sub>3</sub> nanoparticle size and the increase in the luminescent properties. This correlation could be considered somewhat counterintuitive, since the higher surface-to-volume ratio expected for smaller particles could potentially give rise to a higher surface defect concentration per unit

volume, which could partially quench the overall emissive properties. However, previous studies have demonstrated that smaller perovskite particles tend to exhibit higher PLQYs due to quantum confinement effects,<sup>[50]</sup> which minimize the occurrence of non-radiative carrier recombination.<sup>[43,51]</sup> Interestingly, extending the reaction time from 1 to 7 min induces a transition from the weak to the intermediate quantum confinement regime, according to previously reported experimental and theoretical data.<sup>[48]</sup> Therefore, the controlled reduction of the perovskite particle size in the range reported here, achieved by increasing the reaction time, is an effective strategy to enhance the PLQY and, consequently, a means of optimizing the performance of light-emitting devices based on PeNCs. It is worth noting that the data presented from now on will refer only to the PeNCs synthesized after 7 min of reaction, as this material exhibited the best optical properties. Perovskite films were prepared for the sample with 7-min reaction following the same protocol used for the LED films. The PLQY of these films was  $41.1 \pm 2.0\%$  (see Figure S7, Supporting Information).

To deeply investigate the charge carrier recombination characteristics, time-resolved PL (TRPL) measurements were recorded. Figure 2b shows the experimental PL decay (green dotted line) and the fitting (red line) using a triple exponential function. The fitting reveals three time constants ( $\tau_1 = 0.797$  ns,  $\tau_2 = 4.20$  ns, and  $\tau_3 = 21.5$  ns) with different pre-exponential factors, as shown in Table S1, Supporting Information. The obtained average

decay time was 16.5 ns. According to the literature, the fast lifetime component ( $\tau_1$ ) is associated with the direct radiative recombination of excitons in the CsPbBr<sub>3</sub> nanocrystals. The intermediate component ( $\tau_2$ ) is related to defect-assisted recombination, where charge carriers are captured by defects and subsequently recombine. The slow component ( $\tau_3$ ) corresponds to recombination involving deep trap states, where charge carriers are trapped for longer periods before recombining.<sup>[52–55]</sup>

After synthesizing and characterizing the visible light-emitting PeNCs, we meticulously fabricated several batches of PeLEDs, employing CsPbBr<sub>3</sub> NCs as the emissive material, and subjected them to extensive electro-optical characterization. The devices were constructed according to the previously optimized architecture ITO/PEDOT:PSS/poly-TPD/CsPbBr<sub>3</sub> NCs/PO-T2T (40 nm)/LiF (1.0 nm)/Al (100 nm).<sup>[56]</sup> The architecture of our devices was further characterized through SEM (Figure 3a) to visualize the morphology and estimate the thickness of the deposited layers, with their energy level alignment shown in Figure 3b.

Figure 4a displays the electroluminescence (EL) spectra of a PeLED plotted on a logarithmic scale, which reveal a very narrow FWHM of 20 nm and a  $\lambda_{\text{em}}^{\text{max}}$  centered at 516 nm when the device was driven from 4.5 to 7.0 V. Notably, this logarithmic representation allowed us

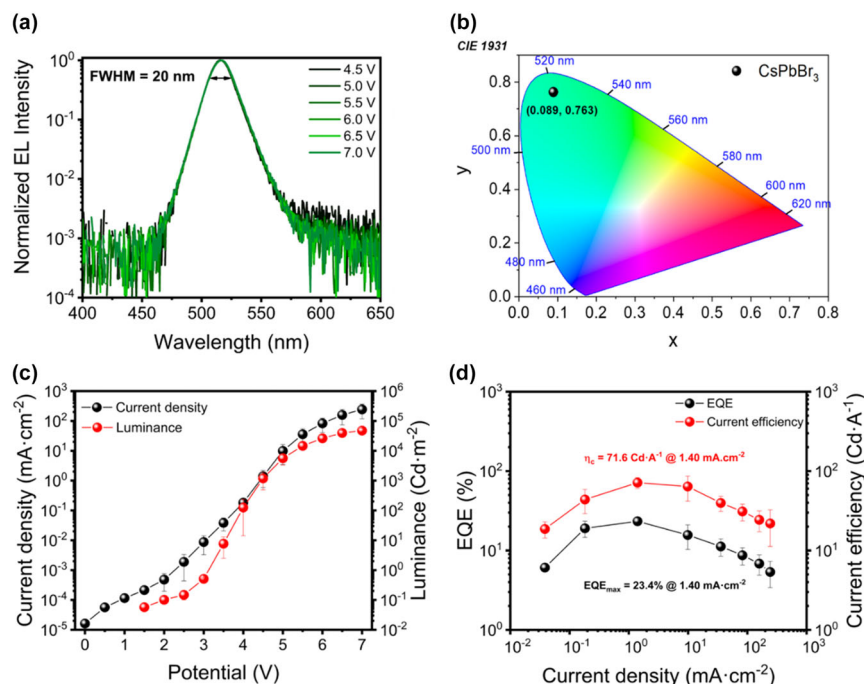


**Figure 4.** Electro-optical characterization of the CsPbBr<sub>3</sub> LEDs: a) EL spectrum recorded at different voltages ( $\lambda_{\text{em}}^{\text{max}} = 516$  nm; FWHM = 20 nm); b) The corresponding *Commission internationale de l'éclairage* (CIE 1931) color coordinates of our LEDs; c) Dependence of the current density ( $I$ ) and Luminance ( $L$ ) versus the applied potential ( $V$ ); d) external quantum efficiency (EQE) and current efficiency ( $\eta_c$ ) plotted versus current density. The different displayed device parameters were obtained upon averaging those values from 30 devices.

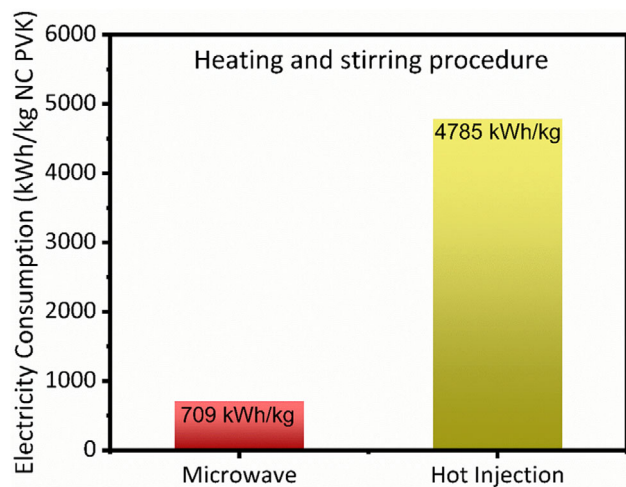


**Figure 5.** Energy consumption of the preparation of PeNCs by MW method compared with HI approach.

to clearly confirm the absence of any parasitic emissions arising from radiative relaxations in other regions of the device, thus reaffirming that the recombination zone is exclusively confined within the ultra-thin and compact PeNCs layer.

As evidenced in Figure 4b, the color coordinates (CIE 1931) extracted from the EL spectrum are located close to the edge of the color space diagram (0.089, 0.763), demonstrating the high purity of the

emitted green light. Additionally, it is worth highlighting the minimal variations in the CIE coordinates ( $x$  and  $y$ ) over time, extracted from the EL spectra under continuous operation of the PeLEDs, even at very high luminance ( $10\,000$  Cd m<sup>-2</sup>), as shown in Figure S8a–c, Supporting Information. This demonstrates the excellent stability of the light characteristics over relatively long functioning periods at different illumination levels.

Our PeLEDs exhibit a low turn-on voltage ( $V_{\text{on}} = 3.0$  V), defined as the potential at a luminance of  $1$  Cd m<sup>-2</sup>,<sup>[57]</sup> which is reasonably close to the bandgap energy of the PeNCs (2.37 eV). This indicates an efficient charge injection (holes and electrons) into the emissive layer, facilitated by the favorable energy level alignment.<sup>[53,58]</sup> Remarkably, the performance parameters corresponding to the PeLEDs shown in Figure 4d demonstrate an average maximum external quantum efficiency (EQE<sub>max</sub>) of  $23.4 \pm 2.8\%$  at a current density of  $1.40$  mA cm<sup>-2</sup> with a corresponding luminance achieved was  $47\,396$  Cd m<sup>-2</sup>. These values represent a significant breakthrough in the exploitation of MW synthesis methodologies for the construction of electro-optical devices, as our devices equal or even outperform the performance of previous PeLEDs based on less efficient and more energy-demanding synthetic methods (Table S2, Supporting Information).

It is worth mentioning that the high performance of our devices is the result of the combination of several crucial factors tackled in our previous contributions:<sup>[47,56,59]</sup> 1) optimized synthetic conditions and the exploitation of exhaustive purification protocols; 2) thorough control over the deposition of the different layers that constitute the LEDs, which includes the choice of suitable charge selective contacts (HTM and ETM, respectively), the fine-tuning of the thicknesses of all the stacked layers with reduced surface roughness, and an appropriate encapsulation of the active areas. This holistic optimization has led to the fabrication of PeLEDs in which the total thickness of the device is lower than 100 nm (excluding the glass substrate, the ITO layer, and the aluminium contact) with very low surface roughness (Figure 3a). On the one hand, the fineness of the CsPbBr<sub>3</sub> layer ( $\approx 20$  nm) ensures a high carrier concentration even at low current densities, which enormously increases the probability of radiative recombination. On the other hand, waveguiding mode loss has been identified in the literature as a major loss channel for PeLEDs due to the high refractive index of perovskite semiconductors,<sup>[60]</sup> and the magnitude of these losses strongly depends on the perovskite layer thickness. Reducing its thickness to a few tens of nanometers while ensuring a very low surface roughness contributes to maximizing the light outcoupling efficiency.

Figure 5 displays an energy consumption analysis comparing our MW approach with a conventional HI method. These measurements include the directly measured energy consumption in our labs and are normalized for the synthesis of 1 kg of nanocrystals, including the processes of heating and stirring. Note that we have not included the energy consumption of the vacuum pump used to generate the inert

conditions during the HI synthesis, as in this particular case, our pump is oversized, which consumes an amount of energy comparable to the overall heating and stirring procedures ( $5755 \text{ kWh kg}^{-1}$ ), and therefore, it would only introduce more noise to the analysis. It is worth mentioning that the introduction of a power-balanced vacuum pump to match the minimum requirements would make the comparison even more favorable to the MW synthesis. A description of this analysis is provided in the [Supporting Information](#).

The results clearly demonstrate that the MW method is at least seven times less energy demanding than the HI method. This analysis highlights the enormous potential of MW synthesis for up-scaling high-performance PeNCs-based devices and specifically for PeLEDs, in contrast to the traditional HI method.

### 3. Conclusion

In summary, this contribution demonstrates for the first time the suitability of an energy-efficient, up-scalable, fast, and reliable synthetic method based on microwave radiation for the fabrication of high-performance PeLEDs. Despite the fact that there still remain a series of surface-related and interfacial phenomena that are not fully understood,<sup>[47,48]</sup> which account for the generally observed limited long-term stability of PeLEDs, we strongly believe that the successful implementation of the simple and efficient MW synthesis of PeNCs represents a promising breakthrough in the field. Therefore, the intricate interplay of surface characteristics, the nature of crystalline defects, and long-term stability must be comprehensively tackled to enable the improvement of the overall performance of PeLEDs. This holistic approach is essential for the successful realization of efficient and stable PeLEDs suitable for practical implementation in optoelectronics.

### 4. Experimental Section

Detailed information related to the synthesis of active electrodes, physicochemical characterization, and electrochemical evaluation of bifunctional electrodes towards UOR and supercapacitor application is provided in Supporting Information.

### Acknowledgements

This work has been partially supported by LUZ PDC2022-133612-100 and PLEDS PID2022-140090B funded by MCIN/AEI and PROMETEO Program from Generalitat Valenciana (Q-Solutions project reference CIPROM/2021/078). B.J.-L. and T.C.A.S. acknowledge the financial support from Universitat Jaume I (project UJI-B2021-50). T.C.A.S. would like to thank Generalitat Valenciana for her PhD contract (GRISOLIAP/2021/096). Serveis Centrals d'Instrumentació Científica (SCIC) from UJI is acknowledged for providing us the instrumental facilities.

### Conflict of interest

The authors declare no conflict of interest.

### Supporting Information

Supporting Information is available from the Wiley Online Library or from the author.

### Keywords

energy materials, light emitting materials, metal halide perovskites, semiconductors, sustainability

Received: May 1, 2024

Revised: May 27, 2024

Published online: June 6, 2024

- [1] D. N. Dirin, L. Protesescu, D. Trummer, I. V. Kochetygov, S. Yakunin, F. Krumeich, N. P. Stadie, M. V. Kovalenko, *Nano Lett.* **2016**, *16*, 5866.
- [2] J. Kang, L. W. Wang, *J. Phys. Chem. Lett.* **2017**, *8*, 489.
- [3] S. Ten Brinck, F. Zaccaria, I. Infante, *ACS Energy Lett.* **2019**, *4*, 2739.
- [4] H. Zhao, H. Chen, S. Bai, C. Kuang, X. Luo, P. Teng, C. Yin, P. Zeng, L. Hou, Y. Yang, L. Duan, F. Gao, M. Liu, *ACS Energy Lett.* **2021**, *6*, 2395.
- [5] X. Mei, D. Jia, J. Chen, S. Zheng, X. Zhang, *Nano Today* **2022**, *43*, 101449.
- [6] T. A. Wani, J. Shamsi, X. Bai, N. Arora, M. I. Dar, *ACS Omega* **2023**, *8*, 17337.
- [7] C. M. Sutter-Fella, Y. Li, M. Amani, J. W. Ager, F. M. Toma, E. Yablonsvitch, I. D. Sharp, A. Javey, *Nano Lett.* **2016**, *16*, 800.
- [8] F. Di Stasio, S. Christodoulou, N. Huo, G. Konstantatos, *Chem. Mater.* **2017**, *29*, 7663.
- [9] K. Chondroudis, D. B. Mitzi, *Chem. Mater.* **1999**, *11*, 3028.
- [10] Z. K. Tan, R. S. Moghaddam, M. L. Lai, P. Docampo, R. Higler, F. Deschler, M. Price, A. Sadhanala, L. M. Pazos, D. Credgington, F. Hanusch, T. Bein, H. J. Snaith, R. H. Friend, *Nat. Nanotechnol.* **2014**, *9*, 687.
- [11] O. A. Jaramillo-Quintero, R. S. Sanchez, M. Rincon, I. Mora-Sero, *J. Phys. Chem. Lett.* **2015**, *6*, 1883.
- [12] K. Lin, J. Xing, L. N. Quan, F. P. G. de Arquer, X. Gong, J. Lu, L. Xie, W. Zhao, D. Zhang, C. Yan, W. Li, X. Liu, Y. Lu, J. Kirman, E. H. Sargent, Q. Xiong, Z. Wei, *Nature* **2018**, *562*, 245.
- [13] L. Li, W. Zheng, Q. Wan, M. Liu, Q. Zhang, C. Zhang, R. Yan, X. Feng, L. Kong, *J. Phys. Chem. C* **2021**, *125*, 3110.
- [14] M. De Franco, M. Cirignano, T. Cavattoni, H. Bahmani Jalali, M. Prato, F. Di Stasio, *Opt. Mater. X* **2022**, *13*, 100124.
- [15] J. Zhang, T. Zhang, Z. Ma, F. Yuan, X. Zhou, H. Wang, Z. Liu, J. Qing, H. Chen, X. Li, S. Su, J. Xie, Z. Shi, L. Hou, C. Shan, *Adv. Mater.* **2023**, *35*, 2209002.
- [16] Q. Wan, W. Zheng, C. Zou, F. Carulli, C. Zhang, H. Song, M. Liu, Q. Zhang, L. Y. Lin, L. Kong, L. Li, S. Brovelli, *ACS Energy Lett.* **2023**, *8*, 927.
- [17] W. Yu, M. Wei, Z. Tang, H. Zou, L. Li, Y. Zou, S. Yang, Y. Wang, Y. Zhang, X. Li, H. Guo, C. Wu, B. Qu, Y. Gao, G. Lu, S. Wang, Z. Chen, Z. Liu, H. Zhou, B. Wei, Y. Liao, L. Zhang, Y. Li, Q. Gong, E. H. Sargent, L. Xiao, *Adv. Mater.* **2023**, *35*, 2301114.
- [18] S. A. Kulkarni, S. G. Mhaisalkar, N. Mathews, P. P. Boix, *Small Methods* **2019**, *3*, 1800231.
- [19] A. A. M. Brown, B. Damodaran, L. Jiang, J. N. Tey, S. H. Pu, N. Mathews, S. G. Mhaisalkar, *Adv. Energy Mater.* **2020**, *10*, 2001349.
- [20] G. B. Nair, S. Tamboli, R. E. Kroon, S. J. Dhoble, H. C. Swart, *J. Alloys Compd.* **2022**, *928*, 167249.
- [21] A. Suhail, A. Saini, S. Beniwal, M. Bag, *J. Phys. Chem. C* **2023**, *127*, 17298.
- [22] H. T. Ramolahloane, G. B. Nair, H. C. Swart, *Mater. Res. Bull.* **2023**, *165*, 112285.
- [23] Y. Tang, P. Wang, R. Wang, H. Yuan, Y. Xin, X. Ren, Q. Chen, H. Yin, *Appl. Surf. Sci.* **2023**, *616*, 156442.
- [24] L. Protesescu, S. Yakunin, M. I. Bodnarchuk, F. Krieg, R. Caputo, C. H. Hendon, R. X. Yang, A. Walsh, M. V. Kovalenko, *Nano Lett.* **2015**, *15*, 3692.
- [25] C. Li, Z. Zang, W. Chen, Z. Hu, X. Tang, W. Hu, K. Sun, X. Liu, W. Chen, *Opt. Express* **2016**, *24*, 15071.
- [26] D. Yan, S. Zhao, H. Wang, Z. Zang, *Photonics Res.* **2020**, *8*, 1086.
- [27] A. F. Gualdrón-Reyes, S. Masi, I. Mora-Seró, *Trends Chem.* **2021**, *3*, 499.
- [28] W. Yu, W. Tu, H. Liu, *Langmuir* **1999**, *15*, 6.
- [29] H. Pan, X. Xu, J. Liu, X. Li, H. Zhang, A. Huang, Z. Xiao, *J. Alloys Compd.* **2021**, *886*, 161248.

- [30] H. Liu, Z. Wu, H. Gao, J. Shao, H. Zou, D. Yao, Y. Liu, H. Zhang, B. Yang, *ACS Appl. Mater. Interfaces* **2017**, *9*, 42919.
- [31] Q. Pan, H. Hu, Y. Zou, M. Chen, L. Wu, D. Yang, X. Yuan, J. Fan, B. Sun, Q. Zhang, *J. Mater. Chem. C Mater.* **2017**, *5*, 10947.
- [32] Y. Li, H. Huang, Y. Xiong, S. V. Kershaw, A. L. Rogach, *Angew. Chem. Int. Ed.* **2018**, *57*, 5833.
- [33] K. Thesika, A. Vadivel Murugan, *Inorg. Chem.* **2020**, *59*, 6161.
- [34] T. C. A. da Silva, C. Fernández-Saiz, R. S. Sánchez, A. F. Gualdrón-Reyes, I. Mora-Seró, B. Julián-López, *J. Solgel Sci. Technol.* **2023**, DOI: [10.1007/s10971-023-06171-1](https://doi.org/10.1007/s10971-023-06171-1).
- [35] V. K. Lamer, R. H. Dinegar, *J. Am. Chem. Soc.* **1950**, *72*, 4847.
- [36] C. Sun, Y. Jiang, L. Zhang, K. Wei, M. Yuan, *ACS Nano* **2023**, *17*, 17600.
- [37] N. Razgoniaeva, M. Yang, P. Garrett, N. Kholmicheva, P. Moroz, H. Eckard, L. Royo Romero, D. Porotnikov, D. Khon, M. Zamkov, *Chem. Mater.* **2018**, *30*, 1391.
- [38] X. M. Lin, C. M. Sorensen, K. J. Klabunde, *J. Nanopart. Res.* **2000**, *2*, 157.
- [39] M. Sakar, S. Balakumar, *J. Photochem. Photobiol. A Chem.* **2018**, *356*, 150.
- [40] Y. Yuan, J. Ni, J. Yin, J. Guan, X. Zhou, Y. Liu, Y. Ding, H. Cai, J. Zhang, *ACS Appl. Mater. Interfaces* **2020**, *12*, 48861.
- [41] Y. Zhang, T. D. Siegler, C. J. Thomas, M. K. Abney, T. Shah, A. De Gortostiza, R. M. Greene, B. A. Korgel, *Chem. Mater.* **2020**, *32*, 5410.
- [42] J. A. Dias, S. H. Santagneli, S. J. L. Ribeiro, Y. Messaddeq, *Sol. RRL* **2021**, *5*, 2100205.
- [43] A. Dey, J. Ye, A. De, E. Debroye, S. K. Ha, E. Bladt, A. S. Kshirsagar, Z. Wang, J. Yin, Y. Wang, L. N. Quan, F. Yan, M. Gao, X. Li, J. Shamsi, T. Debnath, M. Cao, M. A. Scheel, S. Kumar, J. A. Steele, M. Gerhard, L. Chouhan, K. Xu, X. G. Wu, Y. Li, Y. Zhang, A. Dutta, C. Han, I. Vincon, A. L. Rogach, A. Nag, A. Samanta, B. A. Korgel, C. J. Shih, D. R. Gamelin, D. H. Son, H. Zeng, H. Zhong, H. Sun, H. V. Demir, I. G. Scheblykin, I. Mora-Seró, J. K. Stolarczyk, J. Z. Zhang, J. Feldmann, J. Hofkens, J. M. Luther, J. Pérez-Prieto, L. Li, L. Manna, M. I. Bodnarchuk, M. V. Kovalenko, M. B. J. Roeflaers, N. Pradhan, O. F. Mohammed, O. M. Bakr, P. Yang, P. Müller-Buschbaum, P. V. Kamat, Q. Bao, Q. Zhang, R. Krahn, R. E. Galian, S. D. Stranks, S. Bals, V. Biju, W. A. Tisdale, Y. Yan, R. L. Z. Hoyer, L. Polavarapu, *ACS Nano* **2021**, *15*, 10775.
- [44] F. Haydous, J. M. Gardner, U. B. Cappel, *J. Mater. Chem. A* **2021**, *9*, 23419.
- [45] Y. Wang, F. Yang, X. Li, F. Ru, P. Liu, L. Wang, W. Ji, J. Xia, X. Meng, *Adv. Funct. Mater.* **2019**, *29*, 1904913.
- [46] H. M. Ghaithan, Z. A. Alahmed, S. M. H. Qaid, M. Hezam, A. S. Aldwayyan, *ACS Omega* **2020**, *5*, 7468.
- [47] R. S. Sánchez, A. Villanueva-Antolí, A. Bou, M. Ruiz-Murillo, I. Mora-Seró, J. Bisquert, *Adv. Mater.* **2023**, *35*, 2207993.
- [48] J. Butkus, P. Vashishtha, K. Chen, J. K. Gallaher, S. K. K. Prasad, D. Z. Metin, G. Laufersky, N. Gaston, J. E. Halpert, J. M. Hodgkiss, *Chem. Mater.* **2017**, *29*, 3644.
- [49] S. Mannar, P. Mandal, A. Roy, R. Viswanatha, *J. Phys. Chem. Lett.* **2022**, *13*, 6290.
- [50] J. A. Sichert, Y. Tong, N. Mutz, M. Vollmer, S. Fischer, K. Z. Milowska, R. García Cortadella, B. Nickel, C. Cardenas-Daw, J. K. Stolarczyk, A. S. Urban, J. Feldmann, *Nano Lett.* **2015**, *15*, 6521.
- [51] D. K. Sharma, S. Hirata, M. Vacha, *Nat. Commun.* **2019**, *10*, 4499.
- [52] H. Shi, X. Zhang, X. Sun, R. Chen, X. Zhang, *J. Phys. Chem. C* **2019**, *123*, 19844.
- [53] J. Chen, C. Zhang, X. Liu, L. Peng, J. Lin, X. Chen, *Photonics Res.* **2021**, *9*, 151.
- [54] F. Zhang, H. Zhong, C. Chen, X. G. Wu, X. Hu, H. Huang, J. Han, B. Zou, Y. Dong, *ACS Nano* **2015**, *9*, 4533.
- [55] M. A. Becker, R. Vaxenburg, G. Nedelcu, P. C. Sercel, A. Shabaev, M. J. Mehl, J. G. Michopoulos, S. G. Lambrakos, N. Bernstein, J. L. Lyons, T. Stöferle, R. F. Mahrt, M. V. Kovalenko, D. J. Norris, G. Rainò, A. L. Efros, *Nature* **2018**, *553*, 189.
- [56] K. M. M. Salim, E. Hassanabadi, S. Masi, A. F. Gualdrón-Reyes, M. Franckevicius, A. Devižis, V. Gulbinas, A. Fakharuddin, I. Mora-Seró, *ACS Appl. Electron. Mater.* **2020**, *2*, 2525.
- [57] M. Lu, J. Guo, P. Lu, L. Zhang, Y. Zhang, Q. Dai, Y. Hu, V. L. Colvin, W. W. Yu, *J. Phys. Chem. C* **2019**, *123*, 22787.
- [58] J. Kwak, W. K. Bae, D. Lee, I. Park, J. Lim, M. Park, H. Cho, H. Woo, D. Y. Yoon, K. Char, S. Lee, C. Lee, *Nano Lett.* **2012**, *12*, 2362.
- [59] G. Vescio, G. Mathiazhagan, S. González-Torres, J. Sanchez-Diaz, A. Villanueva-Antolí, R. S. Sánchez, A. F. Gualdrón-Reyes, M. Oszajca, F. Linardi, A. Hauser, F. A. Vinocour-Pacheco, W. Żuraw, S. Öz, S. Hernández, I. Mora-Seró, A. Cirera, B. Garrido, *Adv. Eng. Mater.* **2023**, *25*, 2300927.
- [60] L. Zhao, K. M. Lee, K. Roh, S. U. Z. Khan, B. P. Rand, *Adv. Mater.* **2019**, *31*, 1805836.